ADDITIONAL FIGURES

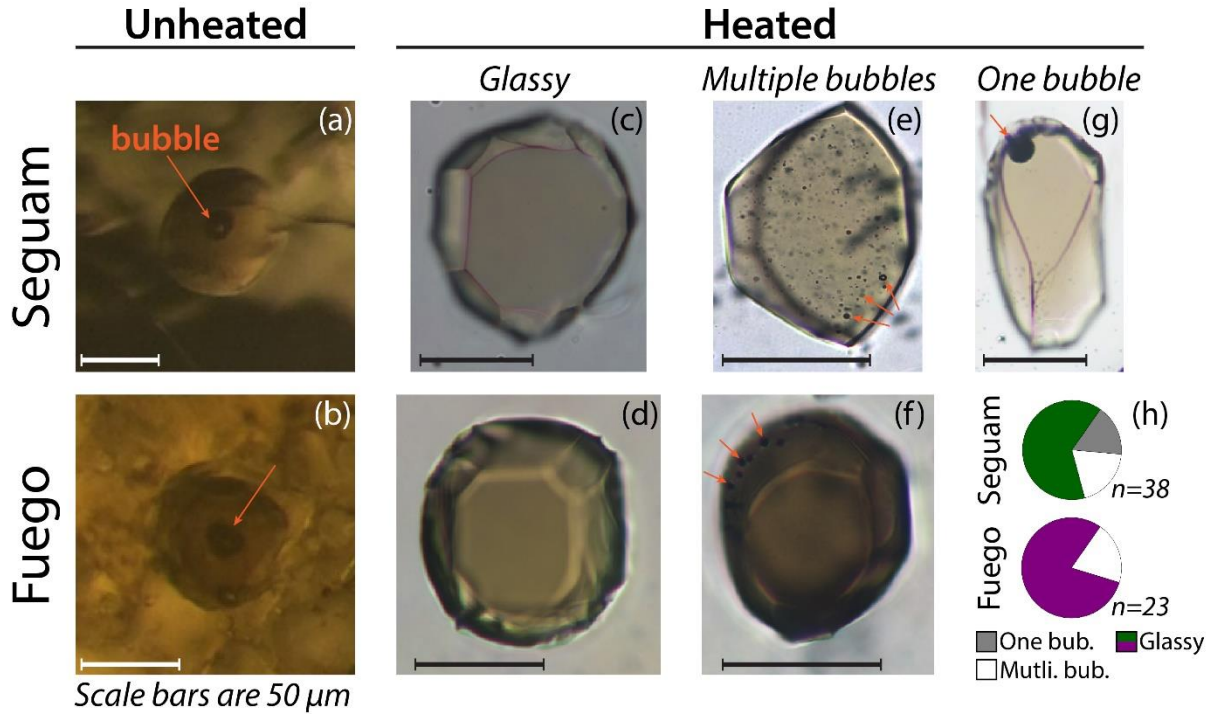

Figure A1. Photomicrographs of melt inclusion vapor bubbles.

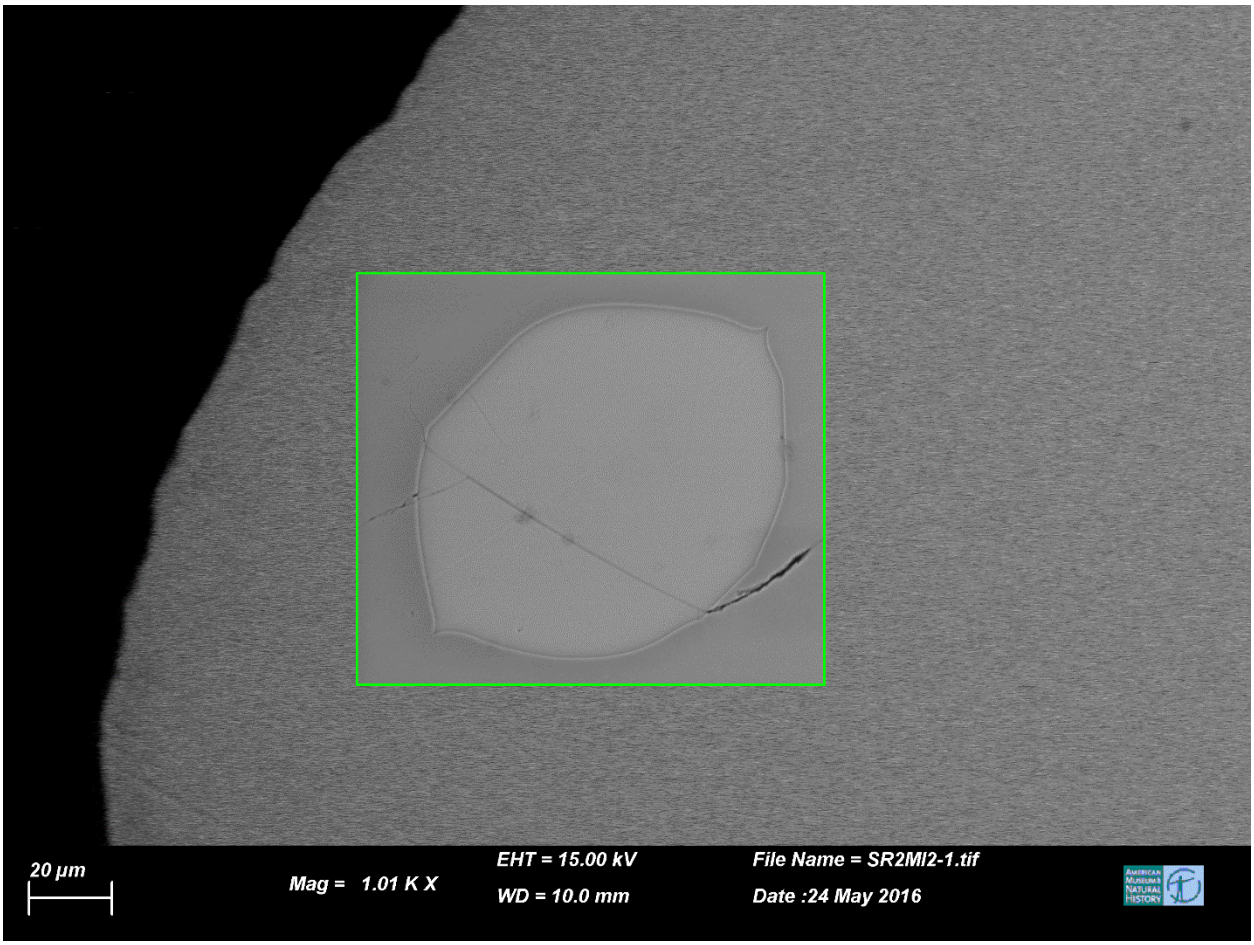

Figure A2. Backscatter electron image of an experimentally rehomogenized melt inclusion (SR02MI02). The dark halo around the melt inclusion has a lower mean atomic number (i.e., higher Fo) than the far field host. This is strong evidence of diffusive gain of Fe (and loss of Mg) in the melt inclusion.

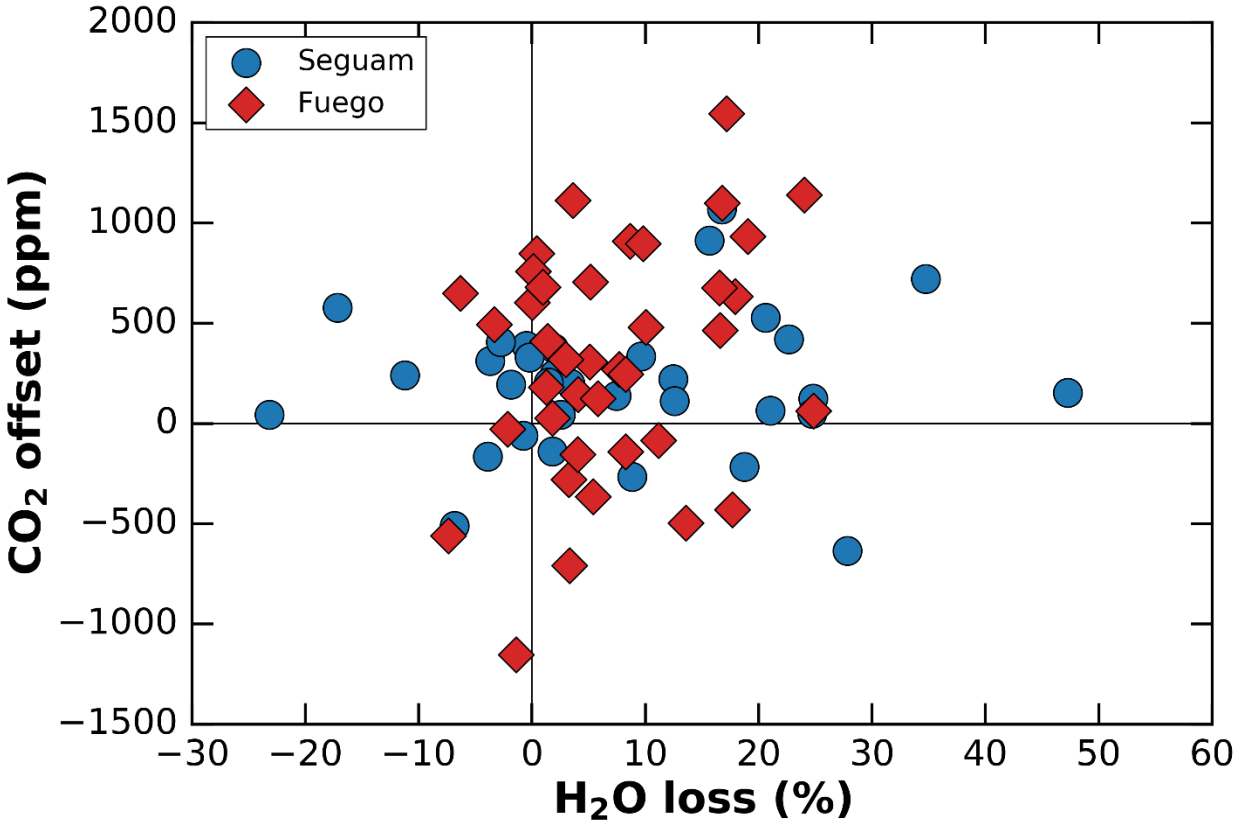

Figure A3. Effect of H_2O loss on reconstructed CO_2 contents. Percent H_2O loss (via diffusive loss of H^+) was calculated with melt inclusion K_2O contents and predicted H_2O-K_2O paths of ascent, degassing, and crystallization (see Appendix 6). CO_2 offset is the difference between the MIMiC-reconstructed CO_2 contents and the CO_2 contents predicted for each melt inclusion using the S-CO_2 degassing path of heated melt inclusions (solid black lines in Fig. 5). Negative values of CO_2 offset indicate MIMiC reconstructions underestimate CO_2 contents, and positive values indicate MIMiC has overestimated CO_2 contents. If H_2O loss was an important consideration in MIMiC CO_2 reconstructions, we would expect that melt inclusions with high values of H_2O loss would have underestimated CO_2 contents (i.e., they would plot in the lower right quadrant). Melt inclusions do not show this.

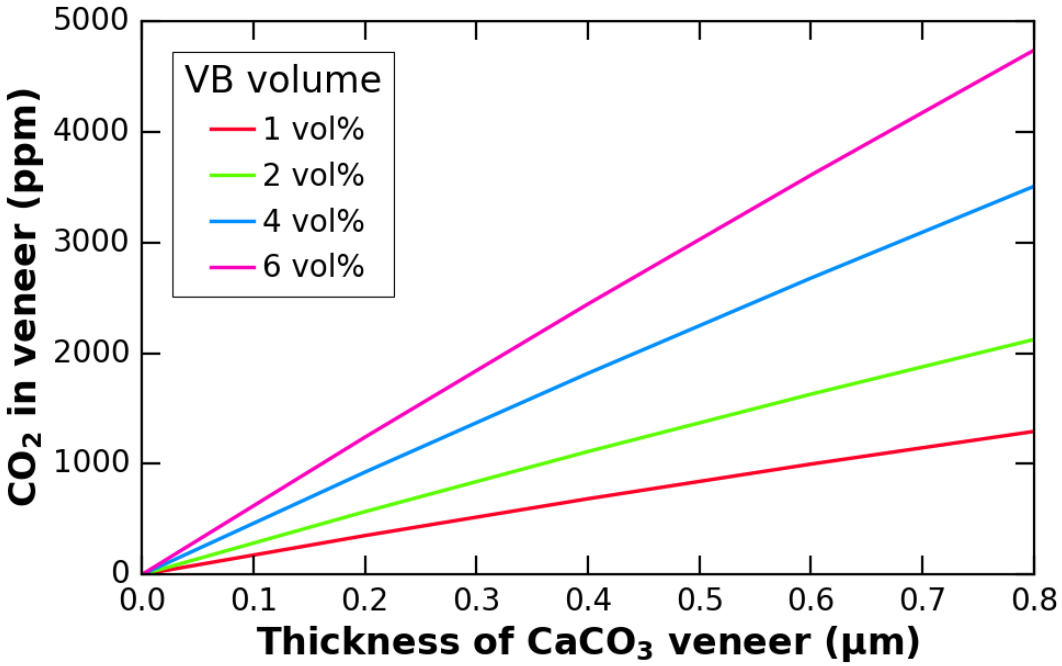

Figure A4. CO_2 content of melt inclusions that could be sequestered in a thin $CaCO_3$ veneer on covering the vapor bubble.